Biophysical Journal Volume 107 December 2014 2734–2743

Article

Systems Mechanobiology: Tension-Inhibited Protein Turnover Is Sufficient to Physically Control Gene Circuits

P. C. Dave P. Dingal[1] and Dennis E. Discher[1,2,*]
[1]Molecular and Cell Biophysics Laboratory, Department of Chemical and Biomolecular Engineering and [2]Graduate Groups in Physics and Cell & Molecular Biology, University of Pennsylvania, Philadelphia, Pennsylvania

ABSTRACT Mechanotransduction pathways convert forces that stress and strain structures within cells into gene expression levels that impact development, homeostasis, and disease. The levels of some key structural proteins in the nucleus, cytoskeleton, or extracellular matrix have been recently reported to scale with tissue- and cell-level forces or mechanical properties such as stiffness, and so the mathematics of mechanotransduction becomes important to understand. Here, we show that if a given structural protein positively regulates its own gene expression, then stresses need only inhibit degradation of that protein to achieve stable, mechanosensitive gene expression. This basic use-it-or-lose-it module is illustrated by application to meshworks of nuclear lamin A, minifilaments of myosin II, and extracellular matrix collagen fibers—all of which possess filamentous coiled-coil/supercoiled structures. Past experiments not only suggest that tension suppresses protein degradation mediated and/or initiated by various enzymes but also that transcript levels vary with protein levels because key transcription factors are regulated by these structural proteins. Coupling between modules occurs within single cells and between cells in tissue, as illustrated during embryonic heart development where cardiac fibroblasts make collagen that cardiomyocytes contract. With few additional assumptions, the basic module has sufficient physics to control key structural genes in both development and disease.

INTRODUCTION

Polymer physics provides fundamental explanations for how elasticity and viscosity of diverse polymer systems often scale as power laws with polymer concentration (1), even when the polymers interact or assemble (2). Living organisms are of course built from biopolymers (Fig. 1 *A*), and assembling proteins such as extracellular matrix (ECM) collagens, which are the most abundant proteins in metazoans, exhibit gel elasticities that indeed scale with concentration when purified and reconstituted (3). Perhaps not surprisingly, tissue stiffness not only scales with collagen levels but is also dictated by the amount of collagen, with soft tissues such as brain having much less collagen than stiffer tissues such as muscle (4). However, biopolymers that include many other key structural proteins within cells and tissues are subject to a variety of enzymatic processes of degradation and synthesis with turnover timescales that, in cell culture, can be only hours or days (5,6). How the mechanics of a tissue or cell reaches or maintains a steady state is therefore a fundamental question of biopolymer physics that impacts the form, function, and dysfunction of cells and tissues in general.

Some of the earliest examples of tension-mediated protein stability were demonstrated in cyclically beating neonatal rat heart cells, where components of the contractile myofibril assembly such as cardiac actin (7) and myosin heavy chain (8) were found degraded when contractile activity was reduced. For collagen fibers, recent evidence suggests mechanical strain stabilizes against enzymatic degradation (9). High matrix stiffness is further associated with an increased stress or tension in the cell (10), and the key contractile protein, myosin II, responds to matrix stiffness by assembling into stress fibers and increasing in amount (11,12). More recently, we have shown that nucleoskeletal lamin-A level scales with tissue microelasticity E, with higher lamin A levels giving physically stiffer nuclei in stiffer tissues (4). Lamin A and myosin II thus seem to mechanically couple to the collagenous matrix (Fig. 1 *A*) in ways that are prescribed by polymer physics. These coiled-coil proteins that assemble into structural networks are prime candidates as biological tension sensors, transducing similar mechanical signals from the ECM to the nucleus (13).

Genome-wide measurements of the production and degradation dynamics of mRNA as well as protein in mouse fibroblasts (NIH 3T3; National Institutes of Health, Bethesda, MD) in standard cultures (5) have shown that mRNA and protein half-lives are fairly uniform within structural groupings of collagens, cytoskeletal and nucleoskeletal components (Fig. 1 *B*). Collagen and actomyosin modules differ significantly in half-lives, and the integrins exhibit intermediate half-lives consistent perhaps with these membrane proteins serving as intermediary linkages between ECM and the cytoskeleton. Even structural proteins on the nuclear envelope such as lamins exhibit largely coordinated expression as a single module, with half-lives

Submitted September 12, 2014, and accepted for publication October 27, 2014.

*Correspondence: discher@seas.upenn.edu

Editor: Sean Sun.

0006-3495/14/12/2734/10 $2.00

http://dx.doi.org/10.1016/j.bpj.2014.10.042

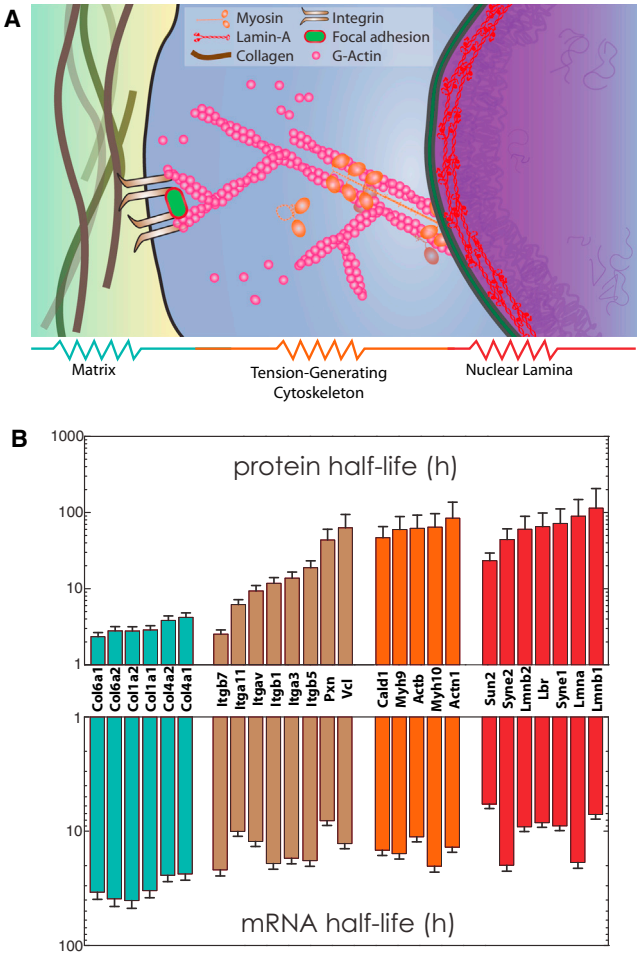

FIGURE 1 Systems-level view of structural molecules involved in mechanotransduction. (*A*) A living cell and its microenvironment are built from biopolymers that provide structure; these molecules assemble and are interconnected, to resist stress arising from development or disease. (*B*) Protein (*top*) and mRNA (*bottom*) half-lives of collagens (*teal*), membrane-bound integrins (*brown*), and cytoskeletal (*orange*) and nuclear envelope components (*red*) measured in NIH3T3 mouse fibroblasts grown on conventional rigid plastic (5). Half-lives are relatively constant within structural groups, suggesting similar dynamics.

similar to those for the actomyosin module. This seems consistent with mechanically coordinated responses of the nuclear lamina to cytoskeletal stresses (14). Much has already been learned from modeling the dependence of structure and dynamics of adhesions and the contractile cytoskeleton on matrix mechanics or forces (15–21). Here we focus on higher-level, long-time models that address mechanics-dependent trends in expression for which experimental data is just beginning to emerge.

GENERAL METHODS

For a given structural gene (S) and its corresponding protein (s) in a module, typical rate equations consist of synthesis and turnover rates such that

$$\frac{dS}{dt} = \alpha(s,\ldots) - \beta(S,\ldots), \tag{1}$$

$$\frac{ds}{dt} = \gamma(S,\ldots) - \delta(s,\ldots), \tag{2}$$

where S and s represent the concentrations of mRNA and protein (dimensionless; normalized to total mRNA and protein levels), respectively, and whose synthesis (α, γ) and degradation (β, δ) rates dictate expression levels. The synthesis rate α is considered to be a function of protein levels (s)—a positive feedback loop that may produce bistability depending on the cooperativity of protein-induced feedback (22), but the new and perhaps important goal of modeling mechanobiology here is to somehow incorporate cell and matrix mechanics into these otherwise classic expressions for α, β, δ, and γ. Any of these rate terms could in principle be functions of S, s and other factors such as matrix elasticity or cell tension. Variations of the rate orders in Eqs. 1 and 2 were explored further in the Supporting Material. Phase plots of gene and protein levels were generated numerically (MATHEMATICA, Ver. 9; Wolfram Research, Champaign, IL) for each variation, and how each rate form could properly recapitulate matrix elasticity-dependence of structural proteins was explored. The goal here is to identify a possible minimal model that fits contemporary understanding of tension coupling to gene expression.

We consider tension-mediated stabilization of polymeric, structural proteins as the basis for systems mechanobiology, and here we explore such models mathematically for single, coupled, and population-coupled modules. Structural proteins of the extracellular matrix, cytoskeleton, or nucleoskeleton are understandably polymeric. In an effort to parsimoniously define a mechanobiological gene circuit, we assume that polymerization and depolymerization rates are relatively rapid compared to the rates defined here. Thus, tension-mediated turnover rate (δ) is assumed to depend simply on effective tension, giving protein concentration, s. Tension on various coiled-coil assemblies has been shown to suppress the affinity of a phosphorylating kinase/protease that initiates enzymatic solubilization/degradation (4,9,23,24). Like pulling on a wet rope to wring out water, tension squeezes out free volume or sterically shields binding sites via coiled-coil assembly to prevent enzyme access. Single-molecule studies of collagen have suggested tension-enhanced degradation (25), but such short polymers tend to unwind under tension, whereas ropelike polymer fibers would tend to tighten their coils and knots. Regardless of mechanism, the rate of degradation can be generally represented by Michaelis-Menten kinetics (26) as

$$\delta(s) = \frac{\delta_0 s^n}{K_s^n + s^n}, \tag{3}$$

where δ_0 is the maximum degradation rate at saturating concentrations of substrate s, such as a coiled-coil protein assembly; K_s is an enzyme affinity for the substrate and is a function of tension; and n is a cooperativity coefficient ≥ 2 that is typical of multimeric interactions. By incorporating Eq. 3 into Eq. 2 and by including an experimentally supported mechanism for transcriptional control, we solve the system of differential equations at steady state and arrive at a relationship between S, s and tension-surrogate K_s. In contrast to a recent modeling study for the kinetics of RNA-interference of focal adhesions that incorporates the effect of force via a varying concentration of Rho (27), the systems-level modeling here generalizes our recent model of tension-stabilized lamin-A (4). This is a first parsimonious approach to incorporating cell tension and matrix stiffness into traditional rate equations for expression changes (Eqs. 1 and 2).

Starting with the model above applied to lamin A, we then extend the model to two structural modules that couple the nucleoskeleton to the cytoskeleton. Dynamics on the tissue-level is then illustrated with a two-cell type model of embryonic heart development. Our models thus elaborate systems-level behavior of structural modules that respond to mechanical stress. These results have implications for both the physiology and pathophysiology of diseases involving structural proteins, from early cardiac development to stress-dependent aging.

The sets of ordinary differential equations that describe the various mechanobiological systems modeled here are explicitly written in the Supporting Material. The analytical results are also derived where applicable. The values of the various rate constants, initial conditions, etc., used in each model are also included in the Supporting Material. Steady-state measurements were obtained by allowing the system to run until the levels of each species stabilize.

RESULTS

Tension-inhibited degradation of coiled-coil proteins

With lamin-A as a representative mechanosensitive protein, we predicted systems-level trends by constructing a parsimonious model of its gene circuit that takes into account protein-mediated feedback on transcription and tension-dependent protein turnover (Fig. 2 *A*). Lamin-A protein is known to feed-back on its own gene through positively regulating its own transcription factor, retinoic acid receptor-γ (RARG) (4). Kinetic measurements of lamin-A changes with mechanical perturbations are clearly needed to further define the model. We found that only first-order rates can sufficiently recapitulate experimental observations. For simplicity, synthesis of messenger RNA (mRNA) and protein as well as degradation of mRNA were all assumed to be linear with rate constants of order unity (to eliminate bias on one biological process), such that the rate equations for lamin-A mRNA (L) and protein (l) are

$$\frac{dL}{dt} = l - 2 \cdot L, \tag{4}$$

$$\frac{dl}{dt} = 3 \cdot L - \frac{4 \cdot l^n}{K_l^n + l^n}. \tag{5}$$

Time evolution of protein (l) and mRNA (L) can be analytically solved with example trajectories in Fig. 2 *B* as a phase plot of $l(t)$ versus $L(t)$ converging to steady-state values: $\{l_{ss}, L_{ss}\}$. Because of how tension-mediated degradation and positive feedback are modeled, the shape of the nullclines allows for the two physiologically relevant steady states. The phase plot shows a stable, nonzero, steady-state node and a saddle point at zero where the mRNA and protein nullclines intersect, lending both mathematical consistency and biophysical relevance to the parsimonious model (further details in the Supporting Material). A set-point tension (K_l) that a cell encounters dictates the magnitude of steady-state levels.

The phase plot also suggests that the initial protein and mRNA levels dictate expression dynamics, and it should be noted that initial states and trajectories include cases where—for example—protein is high and decreasing, whereas transcript is low and increasing in seemingly uncorrelated processes. For example, for lamin A and the nucleoskeletal module, which have stable protein levels but unstable mRNA levels (5), protein dynamics for a given tension set-point (K_l) are predictably well controlled and stabilize linearly toward steady-state (Fig. 2 *B*, *upper-left quadrant*). Lamin A is of course known for tethering heterochromatin near the nuclear envelope, and thus, may need a relatively stable protein expression. Other gene groups with unstable mRNAs include RNA-binding proteins (5). On the other hand, the ECM module has the opposite trend (Fig. 1 *B*); the kinetics of the model predicts that, for highly stable mRNA but short-lived protein levels, the dynamics are nonlinear (Fig. 2 *B*, *lower-right quadrant*). That is, protein levels would overshoot before stabilizing at a steady-state level. The kinetics of this regime was verified by tracking collagen protein expression in mesenchymal stem cells over time from suspension to attachment, starting at low collagen protein levels but with *COL1* mRNA levels remaining relatively stable among structural genes (Fig. 1 *B*). Cell suspension has been known to cease translational rates, and sequester mRNA for subsequent protein synthesis during anchorage recovery (28). With an initially high mRNA level (Fig. 2 *B*, *lower-right quadrant*), collagen protein tended to overshoot before stabilizing at a lower steady-state concentration, as was observed experimentally over seven days (Fig. 2 C). Other gene groups in this

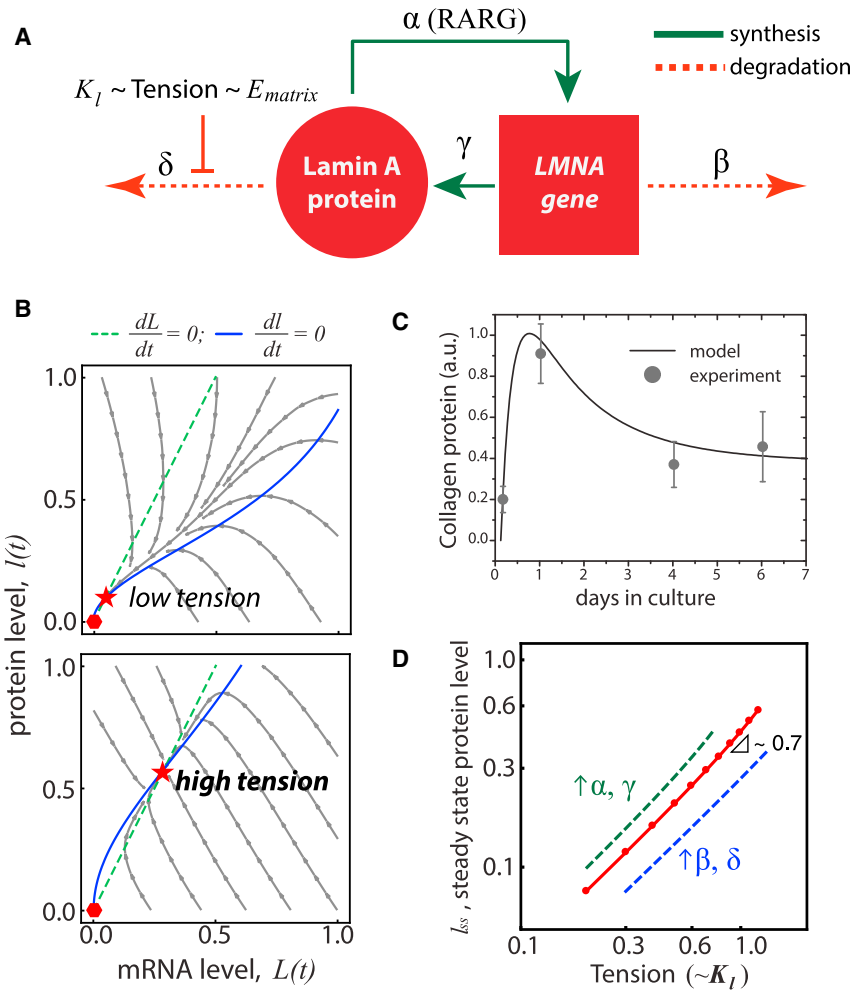

FIGURE 2 Feedback-based mechanobiological gene circuit model for lamin A exhibits polymer-physics scaling if cell tension suppresses protein turnover. (*A*) Nucleoskeletal Lamin-A protein regulates its own message (*LMNA*) and assembles in response to tension from matrix elasticity (E_{matrix}), which inhibits protein degradation. (*B*) Trajectories of lamin-A message and protein as the model converges from a range of initial conditions (*arrowed lines*) to where mRNA (*dashed lines*) and protein (*solid lines*) nullclines intersect to give a stable steady-state solution (star) appropriate to the tension (*top*, $K_l = 0.5$; *bottom*, $K_l = 1.1$). Null solution is unstable (hexagon). (*C*) Procollagen-1 expression in mesenchymal stem cells over seven days was tracked by immunolabeling and quantified. Stem cells adhere and spread on a substrate and start to synthesize collagen matrix, which stabilizes over time. The biphasic kinetic response can be recapitulated by the model that assumes tension-based inhibition of collagen protein degradation rate. (*D*) Setting the kinase/protease binding coefficient, K_l, to be proportional to (Tension)$^{0.3}$ allows the model to generate steady-state scaling with tension that is consistent with tissue-level scaling of lamin A (4). Increasing the synthesis (α, γ) or degradation (β, δ) rates shifts steady-state lamin-A levels higher or lower, respectively. To see this figure in color, go online.

regime include those involved in defense response and homeostasis (5).

Ultimately, the model suggests that tension dictates the expression of structural genes such as nuclear lamin-A regardless of initial conditions, such that at steady state,

$$\frac{dl}{dt} = 0, \quad \frac{dL}{dt} = 0. \tag{6}$$

Equations 4 and 5 can be solved analytically for $n = 2$ to yield nonzero steady-state values for l and L, (details in the Supporting Material)

$$\{l_{ss}, L_{ss}\} = \left\{ \frac{1}{2}\left(\frac{\tilde{\beta}\delta_0}{\tilde{\gamma}\tilde{\alpha}}\right) - \frac{1}{2}\sqrt{\left(\frac{\tilde{\beta}\delta_0}{\tilde{\gamma}\tilde{\alpha}}\right)^2 - 4K_l^2}, \quad \frac{\tilde{\alpha} l_{ss}}{\tilde{\beta}} \right\}. \tag{7}$$

Based on the steady-state analysis above, a solution only exists if

$$\left(\frac{\tilde{\beta}\delta_0}{\tilde{\gamma}\tilde{\alpha}}\right) \geq 2K_l. \tag{8}$$

Although steady-state values depend on the various rate constants, we assumed all to be important and of ~1 (see the Supporting Material) as we focus on K_l: at high stresses where lamin-A assembly is favored, K_l increases so that phosphorylation-mediated lamin-A degradation (24) decreases. Plotting steady-state lamin-A levels l_{ss} against different values for K_l fit a power-law $l_{ss} \sim K_l^2$ (for $n = 2$). As a test of whether such a model could capture key experimental trends, computational results showed that if $K_l = (\text{Tension})^{0.3}$, then $l_{ss} \sim (\text{Tension})^{0.7}$ (Fig. 2 *D*), which parallels the scaling of lamin A with tissue microelasticity E (noting that Tension ~ E) (4). This assumed relationship of K_l and Tension is analogous to the scaling physics of solvent to polymer stability. The set of equations and trends delineated above also applies obviously to collagen because it defines tissue E itself, and it was found to scale more strongly experimentally ($E^{1.5}$) (4).

Mechanical coupling of coiled-coil modules in series

We further developed our model by coupling two coiled-coil proteins in the cytoskeleton and nucleoskeleton modules,

with nonmuscle myosin (e.g., MYH9) and lamin A as representatives in their respective modules. Lamin-A $\{L,l\}$ and nonmuscle-myosin $\{M,\mathrm{m}\}$ message and protein circuitry is schematically presented in Fig. 3 *A*.

In particular, the expression kinetics were described as coupled rate equations for respective transcripts $\{L,M\}$ and proteins $\{l,m\}$:

$$\frac{dL}{dt} = \tilde{\alpha}_1 \cdot l - \tilde{\beta}_1 \cdot L, \tag{9}$$

$$\frac{dl}{dt} = \tilde{\gamma}_1 \cdot L - \underbrace{\delta_1 \cdot \frac{l^{n_l}}{K_l^{n_l} + l^{n_l}}}_{\text{coupled to myosin}}, \tag{10}$$

$$\frac{dM}{dt} = \tilde{\alpha}_2 \cdot m + \tilde{\alpha}_3 \cdot l - \tilde{\beta}_2 \cdot M, \tag{11}$$

$$\frac{dm}{dt} = \tilde{\gamma}_2 \cdot M - \underbrace{\delta_2 \cdot \frac{m^{n_m}}{K_m^{n_m} + m^{n_m}}}_{\text{coupled to matrix } E}. \tag{12}$$

Again, for simplicity, mRNA degradation and translation rates were assumed to be of first-order. Lamin-A protein positively regulates one of its transcription factors (*RARG*; Swift et al. (4)) as does MYH9 with one of its transcription factors (*SRF*; Miralles et al. (29)) so that each enhances its own transcription (with rate constants, $\tilde{\alpha}_1$ and $\tilde{\alpha}_2$, respectively). Mechanical regulation of protein phosphorylation and turnover has been demonstrated in recent studies (4,23,24), and so we described lamin-A and myosin turnover with suitable Hill functions (rate constants δ_1, δ_2). Specifically, lamin-A turnover is dictated by $K_l = m^{x/n_l}$ for some x that dictates sensitivity of lamin-A degradation to myosin-generated

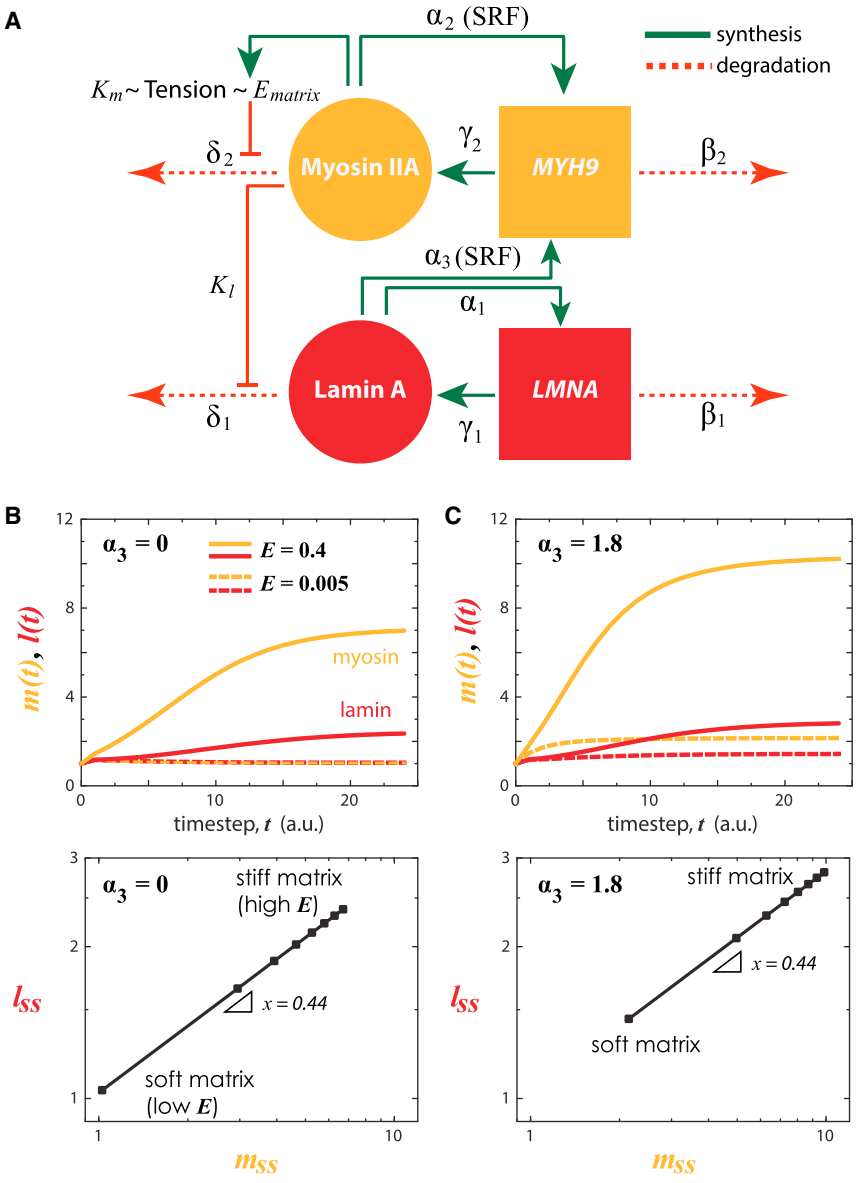

FIGURE 3 Matrix stiffness-coupled lamin A and MYH9 turnover. (*A*) Cytoskeletal myosin and nucleoskeletal lamin A is coupled where each regulates their own message and follows a tension-inhibited degradation mechanism. Lamin A has also been shown to regulate SRF-target genes (α_3), such as *MYH9* (4). (*B*) Kinetics (*top*) and steady-state (*bottom*) myosin (m) and lamin A (l) protein levels, assuming $\alpha_3 = 0$, at low ($E = 0.005$) or high ($E = 0.4$) tension. (*C*) With feedback of lamin A on myosin transcription ($\alpha_3 > 0$), both myosin and lamin levels are increased. To see this figure in color, go online.

stress. Myosin protein turnover is, in turn, dictated by matrix elasticity simply as $K_m = E^{y/n_m}$ for some y that represents the affinity for myosin degradation. Both K_m and K_l effectively couple matrix mechanics to cytoskeletal stress, which in turn tenses the nucleoskeleton (Fig. 1 *A*; Wang et al. (13)).

Equations 9–12 were solved numerically at steady state (all derivatives = 0; see the Supporting Material). Rate constants and free parameters were adjusted collectively within an order of magnitude of each other (see the Supporting Material) to reflect the observed similar half-lives of the modules (Fig. 1 *B*). In the simplest case, we first assumed synthesis and degradation rate constants to be equal,

$$\tilde{\alpha}_1 = \tilde{\alpha}_2,\ \ \tilde{\alpha}_3 = 0,\ \ \tilde{\beta}_1 = \tilde{\beta}_2,\ \ \tilde{\gamma}_1 = \tilde{\gamma}_2,$$
$$n_m = n_l,\ \ \text{and}\ x = y,$$

and observed that, for any given E, the range of expression for myosin is larger than that for lamin A (Fig. 3 *B*). This likely reflects the matrix-cytoskeleton-nucleoskeleton assembly in series (Fig. 1 *A*). Nonetheless, because matrix and cell tension suppresses protein phosphorylation and turnover, steady-state levels monotonically increase with matrix E, consistent with coupled mechanoregulation of lamin A and myosin (24).

If we consider a first-order effect of lamin-A protein on MYH9 transcription via SRF pathway ($\tilde{\alpha}_3$>0; Swift et al. (4)), numerical analysis showed that the dynamic range of myosin increased further due to matrix E and lamin-A contributions, but not the slope of the myosin–lamin-A response to matrix E (Fig. 3 *C*). The relative sensitivity of each module is instead dependent on x and y. If sensitivity of lamin A to degradation (x) is increased (or decreased), then more (lesser) myosin protein is required to generate the same stress that maintains the original lamin-A protein level (Fig. 4 *A*). Increasing x is similar to decoupling nucleoskeletal and cytoskeletal modules, as was done experimentally by ectopic expression of SUN2, a nuclear membrane protein that connects the nucleoskeleton to the cytoskeleton, which led to reduced lamin-A levels (4). On the other hand, if sensitivity of myosin to degradation (y) is decreased, then at low E the steady-state levels of myosin (and indirectly, lamin A) is much higher than at sufficiently high matrix E, where myosin (and lamin) levels remain relatively unperturbed (Fig. 4 *B*). Experiments that observed this prediction include a nonphosphorylatable myosin mutant, which localizes to assembled stress fibers and overrides soft-matrix (low E) effects on stem-cell phenotype; conversely, a phosphomimetic myosin mutant that enriches in the soluble pool fails to completely override stiff-matrix (high E) effects (23).

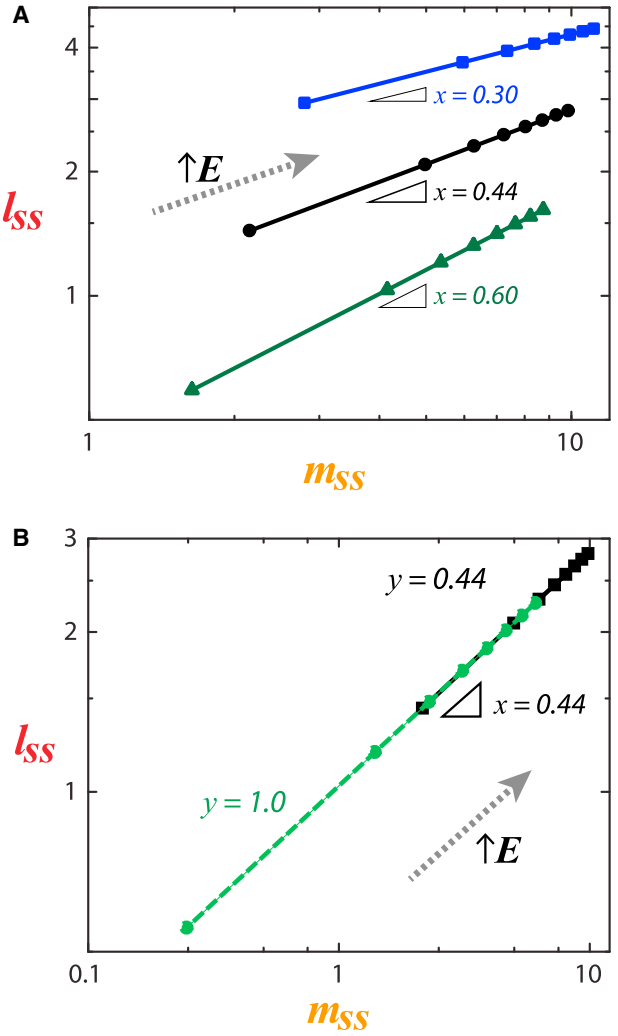

FIGURE 4 Sensitivity analysis of coupled structural modules. (*A*) By varying x, we can perturb the (slope) sensitivity of lamin A to degradation in response to myosin-generated stress. (*B*) Varying y perturbs the degradation sensitivity of myosin, but not its coupling with lamin A. To see this figure in color, go online.

Logistic coupling between collagen and myosin in cardiac development

Systems biology can potentially build an integrated understanding of the electrophysiological and physical processes involved in cardiac physiology and pathophysiology. It might also help identify therapeutic targets. Understanding how the balance between mechanical stiffness and contractile ability of the myocardium is achieved with age and pathological changes, ultimately requires a systems-level model to guide hypotheses. The expression of actomyosin contractility proteins and collagen, among hundreds of abundant proteins, parallel myocardial stiffening in development (30). Both static/cyclic and uniaxial/biaxial strains encourage collagen matrix deposition by cardiac fibroblasts (31), inasmuch as passive and active contraction increase throughout cardiac development. However, as contractility (or myosin levels) increasingly strains the developing heart tissue, we postulate that fibroblast proliferation is ultimately limited by the stiffness of their environment, which correlates strongly with collagen-1 levels (4,30). The various

components of the developing heart matrix and cytoskeleton, and any other functionally relevant signaling proteins, must be integrated into a realistic physical model of the observed mechanics. Thus, we considered using our simplified model that focuses on the mechanical interaction between the collagenous matrix deposited by cardiac fibroblasts and the contractile activity of cardiomyocytes.

To explore possible general mechanisms within the developing myocardium, a coupled network of myosin $\{M,m\}$ and collagen $\{C,c\}$ mRNAs and proteins can be modeled within the developing myocardium (Fig. 5 *A*). With collagen produced primarily by cardiac fibroblasts, the rate of collagen mRNA production is assumed to be proportional to the fibroblast population, which is in turn limited by tissue stiffness imparted by collagen matrix density, such that

$$\frac{dC}{dt} = \underbrace{\tilde{\alpha}_1 \cdot \frac{c^{n_f-1}}{k_f^{n_f} + c^{n_f}}}_{\text{fibroblast crowding}} - \tilde{\beta}_1 \cdot C. \qquad (13)$$

The collagen mRNA production rate of fibroblasts increases at low collagen matrix densities up to a critical collagen

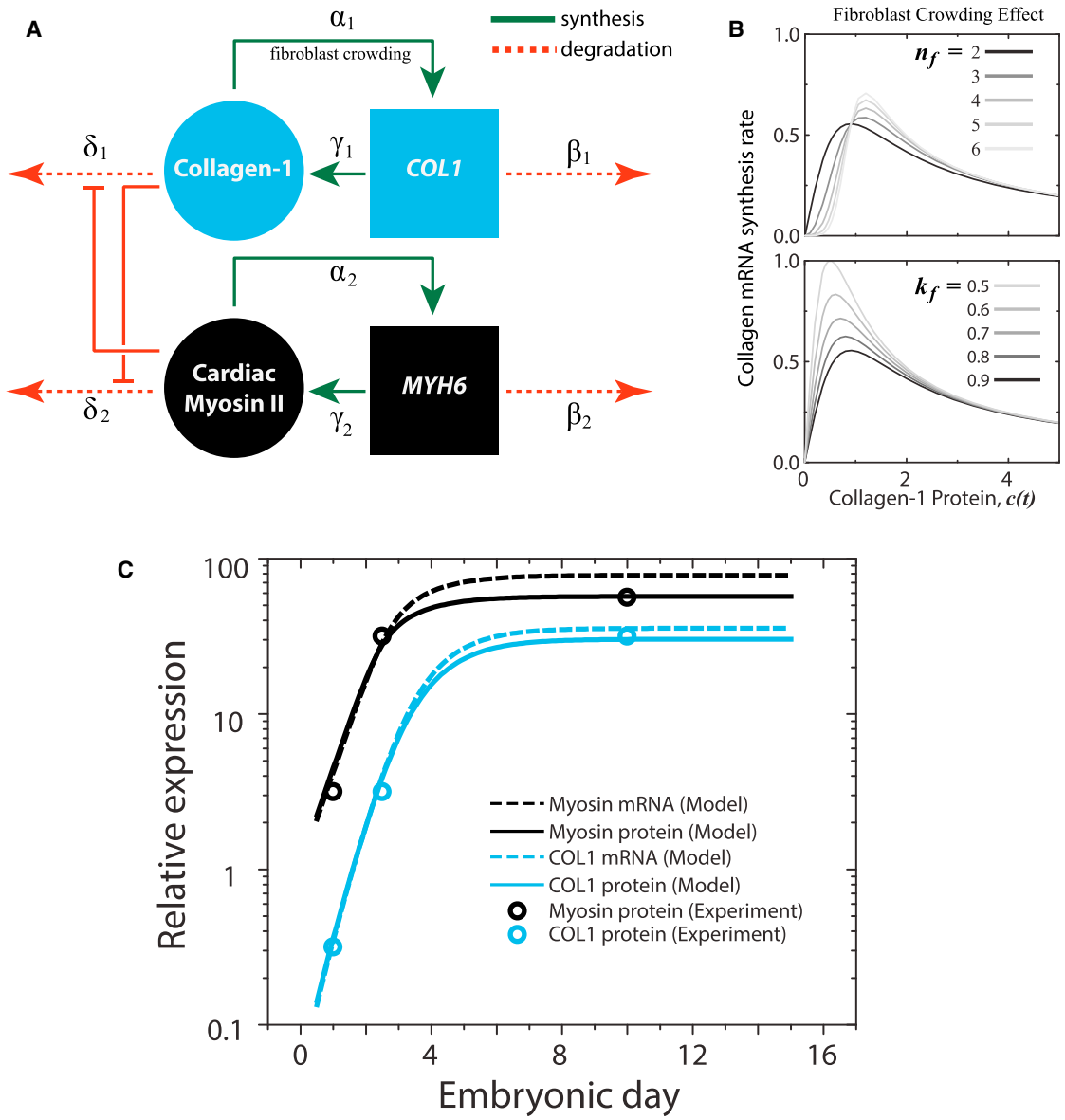

FIGURE 5 Cardiomyocytes and fibroblasts balance contraction and matrix production during heart development. (*A*) Assumptions in matrix stiffness limiting fibroblast population α_1 (and hence, collagen expression), while encouraging myofibril organization in cardiomyocytes (and hence, myosin expression) are incorporated in a model where tension derived from each module inhibits degradation of the other. (*B*) Fibroblast crowding is modeled by a Hill function of collagen protein (and hence tension) (13) with n_f and k_f as the critical point and amplitude, respectively, of the collagen mRNA synthesis rate. (*C*) Experimentally measured changes in both collagen-1 (COL1) and cardiac myosin expression (*circles*) in a developing embryonic chick heart (30) can be recapitulated by the model (protein, *lines*; mRNA, *dashed lines*). To see this figure in color, go online.

concentration (and hence matrix stiffness), then it decreases thereafter; the critical points and amplitudes of this biphasic behavior are modulated by n_f and k_f, respectively (Fig. 5 *B*).

The concept of tension-mediated degradation is again applied here for collagen protein. Collagen matrices have been shown to be stabilized (against degradation) by applied tension (9), such that

$$\frac{dc}{dt} = \tilde{\gamma}_1 \cdot C - \underbrace{\tilde{\delta}_1 \cdot \frac{c^{n_c}}{K_c^{n_c} + c^{n_c}}}_{\text{coupled to myosin}}. \quad (14)$$

Cardiomyocytes are of course the primary contributors of myosin-mediated tension in cardiac tissue, such that $K_c = m^{x/n_c}$ for some x that dictates the extent of myosin-mediated collagen degradation.

Additionally, myosin-II molecules under tension remain assembled and abundant (4,30), with some evidence of tension-suppressed phosphorylation of nonmuscle myosin-II suggesting an intermediate step (23). Striated muscle myosin-II is certainly turned-over in vivo (32), and its disuse probably favors degradation and muscle atrophy. Thus, the transcript (M) and protein (m) rate equations for cardiac myosin are coupled to collagen such that

$$\frac{dM}{dt} = \alpha_2 \cdot m - \beta_2 \cdot M, \quad (15)$$

$$\frac{dm}{dt} = \gamma_2 \cdot M - \underbrace{\delta_2 \cdot \frac{m^{n_m}}{K_m^{n_m} + m^{n_m}}}_{\text{coupled to collagen}}, \quad (16)$$

where $K_m = c^{y/n_m}$, for some y.

With rate constants and free parameters adjusted within an order of magnitude of each other, Eqs. 13–16 were solved numerically (see the Supporting Material) and obtained best-agreement with the reported experimental results. By representing the basic assumptions on fibroblast population crowding (Eq. 13) and tension-stabilized proteins (Eqs. 14 and 16), the model was able to recapitulate the logistic growth kinetics (Fig. 5 *C*) observed experimentally for cardiac myosin and collagen protein levels in a developing heart (30). The model also predicted, perhaps not surprisingly, that mRNA levels should exhibit the same trends as the protein counterparts (Fig. 5 *C*).

DISCUSSION

Cells experience or exert stresses inside and out. Studies that look into cell mechanics responses on timescales of hours or less (e.g., Webster et al. (33)) need to be somehow linked in future work to half-lives of relevant components, which seem to be on much longer timescales, particularly actin-myosin cytoskeleton components with half-lives of 10–100 h (Fig. 1 *B*). Although here we focused on intracellular tension that increases with matrix stiffness E, externally imposed stresses such as shear flow or stretching of cells in tissue can in principle be incorporated into some functional form of $K = f(E, \text{shear stress, cell stretch,}\ldots)$. Experimental measurements of turnover (per Fig. 1 *B*) are clearly needed for these various stress conditions.

The question remains: Should tension facilitate or suppress protein degradation? From an evolutionary standpoint, multicellularity in metazoans is preceded by the appearance of genes necessary for structural organization and intercellular communication. All biomolecules degrade ("dust to dust"), but rates of decomposition of any material also depend in general on both the state of the material and the thermodynamic properties of the environment (e.g., temperature, stress, oxygen, water, etc.). From a biochemical standpoint, it is possible for cleavage sites to be exposed under tension. With purified protein, collagen-I trimers under tension seem to be degraded faster by collagenase (25), whereas collagen fibers under tension are degraded more slowly (9), which is what we assumed here for collagen (Fig. 5 *A*). Within cultured cells, filamin is reportedly regulated by tension-induced degradation, but an autophagy factor (BAG3) that mediates degradation also potently feeds-back on transcription, so that filamin increases with matrix stiffness and cell tension (34). The transcriptional coactivator YAP/TAZ seems to be involved (34), but TAZ is also known to be degraded more so in cells on soft matrices than stiff matrices and also by treatment with inhibitors of Rho, F-actin, and actomyosin tension (35). Detailed molecular mechanisms remain elusive, but for ropelike coiled-coil polymers, tension could sterically or conformationally prevent protease binding to collagen fibers (9) or kinase binding to myosin minifilaments (23) and the lamin-A meshwork (4). Future experimental work on expression dynamics of mechanosensitive proteins would seem likely to benefit from measurements of turnover rates (e.g., Fig. 2 *B*) while systematically varying extracellular stiffness or stress and intracellular tension.

The concept of tension-mediated transcriptional regulation, especially when applied to lamin-A control, also implicates epigenetic silencing of heterochromatin that is typically sequestered by the nuclear lamina. Additionally, the proposed feedforward mechanism to control *LMNA* necessitates another level of regulation of mechanosensing via transcription-factor control (in this case, by RARG that is modulated by soluble retinoid agonists and antagonists (4)). Regardless of mechanism, the turnover and expression of key structural proteins appears to be mechanoregulated.

In the models presented here, membrane-bound integrins were implicitly lumped together (along with matrix and cytoskeleton) in the K-parameter. Overexpressing integrin receptors does not change the ability of a cell to spread, as observed experimentally (36). However, the relative distribution of integrin types with different bond lifetimes (e.g., slip- and catch-bonds) may affect the coupling of

intracellular tension to extracellular stiffness, as suggested recently by theory (27) and experiment (37). On the other hand, perturbations to the linker of nucleoskeleton and cytoskeleton (LINC) complex are understandably more complicated, inasmuch as they physically couple coiled-coil modules of myosin and lamin and influence chromatin architecture (38). Nonetheless, the LINC complex is implicitly included in the x coefficient, inasmuch as it couples cytoskeletal and nucleoskeletal responses. By applying force to nesprin-1, a component of the LINC complex, an isolated nucleus with an intact nuclear lamina stiffens (39).

To date, most experimental techniques in developmental biology fall short of characterizing the systems-level landscape. Our modeling analysis of collagen and myosin levels in cardiac tissue development (Fig. 5) demonstrates that coupled structural modules are sufficient to recapitulate the dynamics of tissue-level architecture. Given the highly interconnected signaling pathways in mammalian biology, our work distills the essential mechanobiological circuits governing not just intracellular but also tissue-level observations into a testable, theoretical framework. The inherent difficulty of detailing these circuits with accurate rate constants and functional forms will be overcome by developing more sophisticated "-omic" approaches.

SUPPORTING MATERIAL

Four sections, two figures, four tables, numerous equations, and two MATHEMATICA routines are available at http://www.biophysj.org/biophysj/supplemental/S0006-3495(14)01128-X.

Support from the AHA Award #14GRNT20490285, NIH (R01-HL124106, R01-HL062352, P01-DK032094, NCATS-8UL1TR000003, P30-DK090969) and NSF (Materials Research Science and Engineering Center) are gratefully acknowledged.

REFERENCES

1. Gennes, P. G. d. 1979. Scaling concepts in polymer physics. Cornell University Press, Ithaca, N.Y.
2. Doi, M., and S. F. Edwards. 1986. The theory of polymer dynamics. Oxford University Press, Oxford, England.
3. Yang, Y. L., L. M. Leone, and L. J. Kaufman. 2009. Elastic moduli of collagen gels can be predicted from two-dimensional confocal microscopy. *Biophys. J.* 97:2051–2060.
4. Swift, J., I. L. Ivanovska, …, D. E. Discher. 2013. Nuclear lamin-A scales with tissue stiffness and enhances matrix-directed differentiation. *Science.* 341:1240104.
5. Schwanhäusser, B., D. Busse, …, M. Selbach. 2011. Global quantification of mammalian gene expression control. *Nature.* 473:337–342.
6. Eden, E., N. Geva-Zatorsky, …, U. Alon. 2011. Proteome half-life dynamics in living human cells. *Science.* 331:764–768.
7. Sharp, W. W., L. Terracio, …, A. M. Samarel. 1993. Contractile activity modulates actin synthesis and turnover in cultured neonatal rat heart cells. *Circ. Res.* 73:172–183.
8. Byron, K. L., J. L. Puglisi, …, A. M. Samarel. 1996. Myosin heavy chain turnover in cultured neonatal rat heart cells: effects of $[Ca^{2+}]_i$ and contractile activity. *Am. J. Physiol.* 271:C01447–C01456.
9. Flynn, B. P., A. P. Bhole, …, J. W. Ruberti. 2010. Mechanical strain stabilizes reconstituted collagen fibrils against enzymatic degradation by mammalian collagenase matrix metalloproteinase 8 (MMP-8). *PLoS ONE.* 5:e12337.
10. Discher, D. E., P. Janmey, and Y. L. Wang. 2005. Tissue cells feel and respond to the stiffness of their substrate. *Science.* 310:1139–1143.
11. Rehfeldt, F., A. E. X. Brown, …, D. E. Discher. 2012. Hyaluronic acid matrices show matrix stiffness in 2D and 3D dictates cytoskeletal order and myosin-II phosphorylation within stem cells. *Integr. Biol. (Camb).* 4:422–430.
12. Engler, A. J., S. Sen, …, D. E. Discher. 2006. Matrix elasticity directs stem cell lineage specification. *Cell.* 126:677–689.
13. Wang, N., J. D. Tytell, and D. E. Ingber. 2009. Mechanotransduction at a distance: mechanically coupling the extracellular matrix with the nucleus. *Nat. Rev. Mol. Cell Biol.* 10:75–82.
14. Houben, F., F. C. S. Ramaekers, …, J. L. V. Broers. 2007. Role of nuclear lamina-cytoskeleton interactions in the maintenance of cellular strength. *Biochim. Biophys. Acta.* 1773:675–686.
15. Wang, N., J. P. Butler, and D. E. Ingber. 1993. Mechanotransduction across the cell surface and through the cytoskeleton. *Science.* 260:1124–1127.
16. Kumar, S., I. Z. Maxwell, …, D. E. Ingber. 2006. Viscoelastic retraction of single living stress fibers and its impact on cell shape, cytoskeletal organization, and extracellular matrix mechanics. *Biophys. J.* 90:3762–3773.
17. Paul, R., P. Heil, …, U. S. Schwarz. 2008. Propagation of mechanical stress through the actin cytoskeleton toward focal adhesions: model and experiment. *Biophys. J.* 94:1470–1482.
18. Chan, C. E., and D. J. Odde. 2008. Traction dynamics of filopodia on compliant substrates. *Science.* 322:1687–1691.
19. Walcott, S., and S. X. Sun. 2010. A mechanical model of actin stress fiber formation and substrate elasticity sensing in adherent cells. *Proc. Natl. Acad. Sci. USA.* 107:7757–7762.
20. Maître, J. L., H. Berthoumieux, …, C. P. Heisenberg. 2012. Adhesion functions in cell sorting by mechanically coupling the cortices of adhering cells. *Science.* 338:253–256.
21. Novikova, E. A., and C. Storm. 2013. Contractile fibers and catch-bond clusters: a biological force sensor? *Biophys. J.* 105:1336–1345.
22. Griffith, J. S. 1968. Mathematics of cellular control processes. II. Positive feedback to one gene. *J. Theor. Biol.* 20:209–216.
23. Raab, M., J. Swift, …, D. E. Discher. 2012. Crawling from soft to stiff matrix polarizes the cytoskeleton and phosphoregulates myosin-II heavy chain. *J. Cell Biol.* 199:669–683.
24. Buxboim, A., J. Swift, …, D. E. Discher. 2014. Matrix elasticity regulates lamin-A,C phosphorylation and turnover with feedback to actomyosin. *Curr. Biol.* 24:1909–1917.
25. Adhikari, A. S., J. Chai, and A. R. Dunn. 2011. Mechanical load induces a 100-fold increase in the rate of collagen proteolysis by MMP-1. *J. Am. Chem. Soc.* 133:1686–1689.
26. Michaelis, L., and M. L. Menten. 1913. The kinetics of effective invertin [Die kinetik der invertinwirkung]. *Biochem. Z.* 49:333–369.
27. Hoffmann, M., and U. S. Schwarz. 2013. A kinetic model for RNA-interference of focal adhesions. *BMC Syst. Biol.* 7:2.
28. Benecke, B. J., A. Ben-Ze'ev, and S. Penman. 1978. The control of mRNA production, translation and turnover in suspended and reattached anchorage-dependent fibroblasts. *Cell.* 14:931–939.
29. Miralles, F., G. Posern, …, R. Treisman. 2003. Actin dynamics control SRF activity by regulation of its coactivator MAL. *Cell.* 113:329–342.
30. Majkut, S., T. Idema, …, D. E. Discher. 2013. Heart-specific stiffening in early embryos parallels matrix and myosin expression to optimize beating. *Curr. Biol.* 23:2434–2439.

31. MacKenna, D., S. R. Summerour, and F. J. Villarreal. 2000. Role of mechanical factors in modulating cardiac fibroblast function and extracellular matrix synthesis. *Cardiovasc. Res.* 46:257–263.

32. Ball, R. D., D. L. Krus, and B. Alizadeh. 1987. Myosin degradation fragments in skeletal muscle. *J. Mol. Biol.* 193:47–56.

33. Webster, K. D., W. P. Ng, and D. A. Fletcher. 2014. Tensional homeostasis in single fibroblasts. *Biophys. J.* 107:146–155.

34. Ulbricht, A., F. J. Eppler, …, J. Höhfeld. 2013. Cellular mechanotransduction relies on tension-induced and chaperone-assisted autophagy. *Curr. Biol.* 23:430–435.

35. Dupont, S., L. Morsut, …, S. Piccolo. 2011. Role of YAP/TAZ in mechanotransduction. *Nature*. 474:179–183.

36. Engler, A., L. Bacakova, …, D. Discher. 2004. Substrate compliance versus ligand density in cell on gel responses. *Biophys. J.* 86: 617–628.

37. Schiller, H. B., M. R. Hermann, …, R. Fässler. 2013. β1- and αv-class integrins cooperate to regulate myosin II during rigidity sensing of fibronectin-based microenvironments. *Nat. Cell Biol.* 15:625–636.

38. Dahl, K. N., A. J. S. Ribeiro, and J. Lammerding. 2008. Nuclear shape, mechanics, and mechanotransduction. *Circ. Res.* 102:1307–1318.

39. Guilluy, C., L. D. Osborne, …, K. Burridge. 2014. Isolated nuclei adapt to force and reveal a mechanotransduction pathway in the nucleus. *Nat. Cell Biol.* 16:376–381.

Systems Mechano-Biology: Tension-inhibited Protein Turnover is sufficient to physically control Gene Circuits

Supporting Material

P. C. Dave P. Dingal[1] and Dennis E. Discher[1]

[1]Molecular and Cell Biophysics Laboratory, Department of Chemical and Biomolecular Engineering, University of Pennsylvania, Philadelphia, Pennsylvania

Email: P. C. Dave P. Dingal - polimyr@seas.upenn.edu; Dennis E. Discher - discher@seas.upenn.edu

Contents

1 Mechanobiological gene circuit: systems of ordinary differential equations

1.1 Single-module gene circuits: reaction-order stability

A single module refers to a particular gene (S) and its corresponding protein (s) and is described by general rate equations that define what factors affects synthesis and turnover. To incorporate the stabilizing effect of tension (K_s) on protein we define degradation term δ as a Hill function as in Equation **(3)** in the main text:

$$\delta(s) = \frac{\delta_0 s^n}{K_s^n + s^n}$$

The set of ordinary differential equations (ODEs) for a single module is simply:

$$\begin{aligned}\frac{dS}{dt} &= \alpha(s) - \beta(S) \\ \frac{ds}{dt} &= \gamma(S) - \frac{\delta_0 s^n}{K_s^n + s^n}\end{aligned}$$

Ultimately, the value of K_s (and hence, E) dictates the steady state values, regardless of the initial condition. Here, we explored the functional forms of the various rates that dictate the stability and dynamics of the system. For the given Hill-functional form of δ above, we explored the various reaction-order forms of the other rates that converge to a steady state solution.

1.1.1 Rate-order forms by Schwanhausser *et al.*

Schwanhausser *et al.* [1] quantified proteomic and transcriptomic half-lives under the following rate equations:

$$\begin{aligned}\frac{dS}{dt} &= \tilde{\alpha} - \tilde{\beta} \cdot S \\ \frac{ds}{dt} &= \tilde{\gamma} \cdot S - \tilde{\delta} \cdot s\end{aligned}$$

where $\tilde{\alpha}, \tilde{\beta}, \tilde{\gamma}, \tilde{\delta}$ are rate constants. A phase plot of protein (s) and mRNA (S), while varying the ratio of synthesis/degradation rates for protein ($\tilde{\gamma}/\tilde{\delta}$) and mRNA ($\tilde{\alpha}/\tilde{\beta}$), shows that mRNA-relevant rates scale with mRNA and protein levels (blue line), but that the protein-relevant rates do not (red line). This was expected from the chosen forms of the rate equations above where

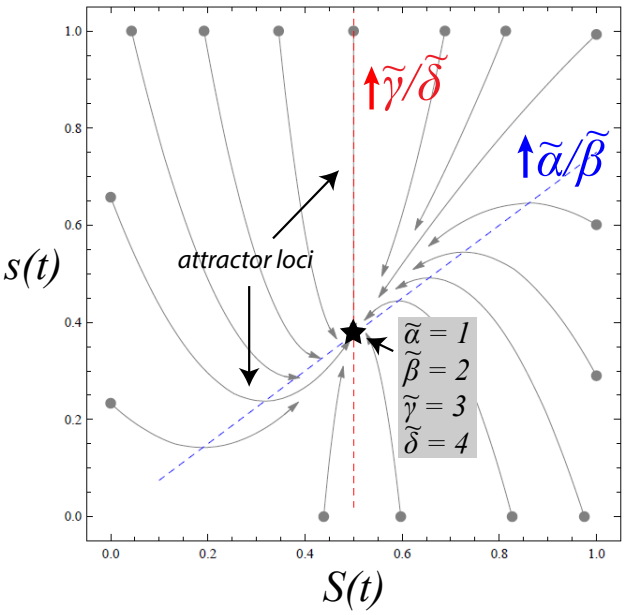

protein levels do not affect mRNA levels. Thus, in the search for the appropriate forms of the rate equations that capture the variations in structural protein expression with matrix elasticity, E, the ones described by Schwanhausser *et al.* are not sufficient.

1.1.2 Zeroth-order α, tension-dependent δ

Now if we consider changing degradation rate to be tension-dependent, keeping others similar to above:

$$\frac{dS}{dt} = \tilde{\alpha} - \tilde{\beta} \cdot S$$
$$\frac{ds}{dt} = \tilde{\gamma} \cdot S - \frac{\delta_0 s^n}{K_s^n + s^n}$$

In this case, we get the following phase plot where varying K_s, and hence protein levels, does not affect mRNA levels. This is again not physically relevant as we expect that both mRNA

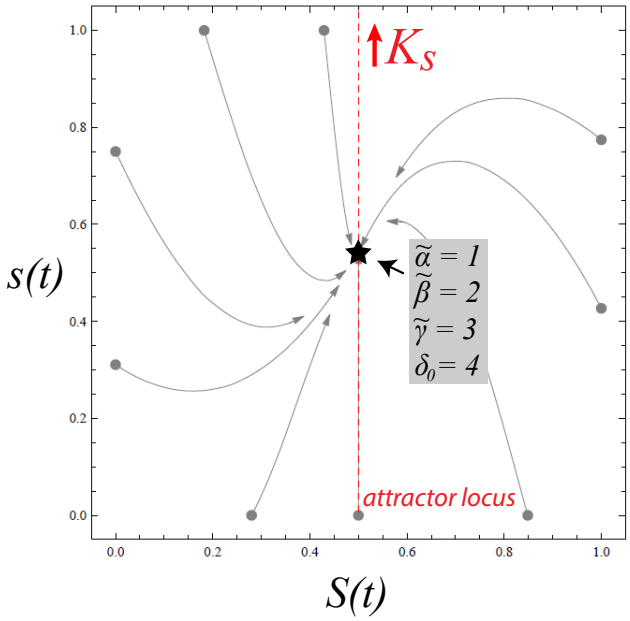

and protein levels should respond to K_s (or E).

1.1.3 First-order rates, tension-dependent δ

First-order rates were chosen for the main text as they parsimoniously recapitulate experimental observations for the mechanobiological gene circuit of lamin A [2].

$$\frac{dS}{dt} = \tilde{\alpha} \cdot s - \tilde{\beta} \cdot S$$
$$\frac{ds}{dt} = \tilde{\gamma} \cdot S - \frac{\delta_0 s^n}{K_s^n + s^n}$$

With the lack of precise values for rate constants published in literature, we chose $O(1)$ values for the parameters. For the purposes of display in Figure 2 of the main text, we used the following values for each of the rate constants:

Parameter	Value
$\tilde{\alpha}$	1 s^{-1}
$\tilde{\beta}$	2 s^{-1}
$\tilde{\gamma}$	3 s^{-1}
δ_0	4 s^{-1}
n	2

For $n = 2$, constraints to rate-parameter values arise and can expressed in analytical form (see Section 2). Protein and mRNA levels were initialized in the range $\{0, 1\}$, as shown in the phase plot in Figure 2B.

1.1.4 Unstable steady states: higher-order rates

The following higher-order ($p \geq 2$) cases exhibit divergent steady states, and hence not biologically relevant:

- $\alpha = \tilde{\alpha} \cdot s^p$; $\beta = \tilde{\beta} \cdot S$; $\gamma = \tilde{\gamma} \cdot S$;
- $\alpha = \tilde{\alpha} \cdot s$; $\beta = \tilde{\beta} \cdot S$ $\gamma = \tilde{\gamma} \cdot S^p$;
- $\alpha = \tilde{\alpha} \cdot s^p$; $\beta = \tilde{\beta} \cdot S^p$ $\gamma = \tilde{\gamma} \cdot S^p$;

1.2 Two-Module Gene Circuit

Assuming first-order rates (except for protein degradation rates), the set of ODEs for coupled two-module gene circuit is:

$$\begin{aligned}
\frac{dL}{dt} &= \tilde{\alpha}_1 \cdot l - \tilde{\beta}_1 \cdot L \\
\frac{dl}{dt} &= \tilde{\gamma}_1 \cdot L - \delta_1 \cdot \frac{l^{n_l}}{K_l^{n_l} + l^{n_l}} \\
\frac{dM}{dt} &= \tilde{\alpha}_2 \cdot m \ \ + \tilde{\alpha}_3 \cdot l - \tilde{\beta}_2 \cdot M \\
\frac{dm}{dt} &= \tilde{\gamma}_2 \cdot M - \delta_2 \cdot \frac{m^{n_m}}{K_m^{n_m} + m^{n_m}}
\end{aligned}$$

where $K_s = f(s)$ or $K_s = f(tension)$ of some functional form (e.g. power-law). For lamin-myosin coupling, we chose $K_l = m^{x/n_l}$ and $K_m = E^{y/n_m}$.

The following values for rate constants were used in the simulations presented in Figures 3B, C of the main text:

Parameter	Value
$\{\tilde{\alpha_1}, \tilde{\alpha_2}\}$	$\{1.1\ s^{-1}, 1.1\ s^{-1}\}$
$\{\tilde{\beta}_1, \tilde{\beta}_2\}$	$\{5\ s^{-1}, 5\ s^{-1}\}$
$\{\tilde{\gamma_1}, \tilde{\gamma_2}\}$	$\{1.2\ s^{-1}, 1.2\ s^{-1}\}$
$\{\delta_1, \delta_2\}$	$\{5\ s^{-1}, 5\ s^{-1}\}$
$\{n_l, n_m\}$	$\{2, 2\}$
$\{x, y\}$	$\{0.44, 0.44\}$

with $E = 0.003 - 0.4$, to represent the order-of-magnitude range of elasticities in cell-on-gel experiments ($0.3 - 40$ kPa; ref. 2). The different molecular species were all initialized as $L(0) = l(0) = m(0) = M(0) = 0.005$.

1.3 Two-Module, Tissue-level Mechanobiological Gene Circuit

The set of ODEs for population-level coupling of two modules (e.g. collagen and myosin levels in a developing heart) are:

$$\begin{aligned}
\frac{dC}{dt} &= \tilde{\alpha}_1 \cdot \frac{c^{n_f-1}}{k_f^{n_f} + c^{n_f}} - \tilde{\beta}_1 \cdot C \\
\frac{dc}{dt} &= \tilde{\gamma}_1 \cdot C - \tilde{\delta}_1 \cdot \frac{c^{n_c}}{K_c^{n_c} + c^{n_c}} \\
\frac{dM}{dt} &= \tilde{\alpha}_2 \cdot m - \tilde{\beta}_2 \cdot M \\
\frac{dm}{dt} &= \tilde{\gamma}_2 \cdot M - \delta_2 \cdot \frac{m^{n_m}}{K_m^{n_m} + m^{n_m}}
\end{aligned}$$

where $K_c = m^{x/n_c}$ for some x, $K_m = c^{y/n_m}$, for some y.

The following values for rate constants were used in the simulations in Figure 5 (unless otherwise specified):

Parameter	Value
$\{\tilde{\alpha_1}, \tilde{\alpha_2}\}$	$\{5.2\ s^{-1}, 4.1\ s^{-1}\}$
$\{\tilde{\beta}_1, \tilde{\beta}_2\}$	$\{5\ s^{-1}, 3\ s^{-1}\}$
$\{\tilde{\gamma_1}, \tilde{\gamma_2}\}$	$\{3\ s^{-1}, 1.5\ s^{-1}\}$
$\{\delta_1, \delta_2\}$	$\{6.5\ s^{-1}, 7\ s^{-1}\}$
$\{n_f, n_c, n_m\}$	$\{2, 1.6, 3.7\}$
$\{x, y, k_f\}$	$\{0.51, 0.39, 0.89\}$

The different molecular species were initialized with the following values:

Species	Initial Value
C	0.00051
c	0.00051
M	0.011
m	0.011

2 Analytical Solution for Single-Module Gene Circuit

For the case that δ is tension-dependent and all other rates are first-order (Section 1.1.3), as in the main text, at steady state we have:

$$F(s,S) = \frac{dS}{dt} = 0 = \tilde{\alpha} \cdot s - \tilde{\beta} \cdot S \tag{2.0.1}$$

$$G(s,S) = \frac{ds}{dt} = 0 = \tilde{\gamma} \cdot S - \frac{\delta_0 s^n}{K_s^n + s^n} \tag{2.0.2}$$

2.1 Stability Analysis

First, we characterize the stability of fixed points (steady-state solutions) in the general case. The set of ODEs above include a nonlinear term, and so we perform linearization near a critical point (s^*, S^*) such that:

$$\begin{pmatrix} S \\ s \end{pmatrix}' = \begin{pmatrix} \frac{\partial F}{\partial S}(s^*,S^*) & \frac{\partial F}{\partial s}(s^*,S^*) \\ \frac{\partial G}{\partial S}(s^*,S^*) & \frac{\partial G}{\partial s}(s^*,S^*) \end{pmatrix} \cdot \begin{pmatrix} S - S^* \\ s - s^* \end{pmatrix}$$

The Jacobian matrix above simplifies to:

$$\begin{pmatrix} -\tilde{\beta} & \tilde{\alpha} \\ \tilde{\gamma} & \delta_0 \frac{nK_s^n (s^*)^{n-1}}{(K_s^n + (s^*)^n)^2} \end{pmatrix}$$

All solutions converge to the critical point when the eigenvalues (λ's) are all negative. The characteristic polynomial of the Jacobian matrix is:

$$\lambda^2 + \left[\tilde{\beta} + \delta_0 \frac{nK_s^n (s^*)^{n-1}}{(K_s^n + (s^*)^n)^2}\right] \cdot \lambda + \left[\tilde{\beta} \cdot \delta_0 \frac{nK_s^n (s^*)^{n-1}}{(K_s^n + (s^*)^n)^2} - \tilde{\gamma}\tilde{\alpha}\right] = 0 \tag{2.1.1}$$

The eigenvalues are:

$$\lambda_{1,2} = -\frac{1}{2}\left[\tilde{\beta} + \delta_0 \frac{nK_s^n (s^*)^{n-1}}{(K_s^n + (s^*)^n)^2}\right] \pm \frac{1}{2}\sqrt{\left[\tilde{\beta} + \delta_0 \frac{nK_s^n (s^*)^{n-1}}{(K_s^n + (s^*)^n)^2}\right]^2 - 4\left[\tilde{\beta} \cdot \delta_0 \frac{nK_s^n (s^*)^{n-1}}{(K_s^n + (s^*)^n)^2} - \tilde{\alpha}\tilde{\gamma}\right]} \tag{2.1.2}$$

In order to obtain a stable steady-state solution, the root term has to be less than the first term for the eigenvalues to be negative:

$$\left[\tilde{\beta} + \delta_0 \frac{nK_s^n (s^*)^{n-1}}{(K_s^n + (s^*)^n)^2}\right]^2 > \left[\tilde{\beta} + \delta_0 \frac{nK_s^n (s^*)^{n-1}}{(K_s^n + (s^*)^n)^2}\right]^2 - 4\left[\tilde{\beta} \cdot \delta_0 \frac{nK_s^n (s^*)^{n-1}}{(K_s^n + (s^*)^n)^2} - \tilde{\gamma}\tilde{\alpha}\right] \tag{2.1.3}$$

Simplifying, we get:

$$\frac{\tilde{\beta}\delta_0}{\tilde{\gamma}\tilde{\alpha}} > \frac{(K_s^n + (s^*)^n)^2}{nK_s^n (s^*)^{n-1}} \tag{2.1.4}$$

Thus, the parameter space of the rate constants must obey the above relationship with tension K_s and steady-state protein level s^*. One can immediately see that the null solution ($s^* = 0$) leads to non-negative eigenvalues, and hence an unstable steady state.

2.2 Steady-state solutions for $n = 2$ case

For the simplest case of $n = 2$ and substituting Eq. (2.0.2) to Eq. (2.0.1), we get (after removing null solution):

$$s^3 - \frac{\tilde{\beta}\delta_0}{\tilde{\gamma}\tilde{\alpha}} s^2 + \tilde{\gamma} K_s^2 s = 0 \tag{2.2.1}$$

$$s^2 - \frac{\tilde{\beta}\delta_0}{\tilde{\gamma}\tilde{\alpha}} s + \tilde{\gamma} K_s^2 = 0 \tag{2.2.2}$$

Equation (2.2.2) is simply a quadratic equation, which has two solutions:

$$s_{1,2} = \frac{1}{2}\left(\frac{\tilde{\beta}\delta_0}{\tilde{\gamma}\tilde{\alpha}}\right) \pm \frac{1}{2}\sqrt{\left(\frac{\tilde{\beta}\delta_0}{\tilde{\gamma}\tilde{\alpha}}\right)^2 - 4K_s^2} \tag{2.2.3}$$

Stability analysis shows that the larger solution does not satisfy Equation (2.1.4) and is an unstable node, such that we only have one biologically relevant, non-zero steady state:

$$\{s_{ss}, S_{ss}\} = \left\{\frac{1}{2}\left(\frac{\tilde{\beta}\delta_0}{\tilde{\gamma}\tilde{\alpha}}\right) - \frac{1}{2}\sqrt{\left(\frac{\tilde{\beta}\delta_0}{\tilde{\gamma}\tilde{\alpha}}\right)^2 - 4K_s^2}, \quad \frac{\tilde{\alpha}s_{ss}}{\tilde{\beta}}\right\} \tag{2.2.4}$$

where the rate constants must have values that obey the following:

$$\left(\frac{\tilde{\beta}\delta_0}{\tilde{\gamma}\tilde{\alpha}}\right)^2 - 4K_s^2 \geq 0 \tag{2.2.5}$$

or simply

$$\left(\frac{\tilde{\beta}\delta_0}{\tilde{\gamma}\tilde{\alpha}}\right) \geq 2K_s \tag{2.2.6}$$

It must be noted that Equation (2.2.6) can also be derived from Equation (2.1.4), when the smaller steady-state solution is used.

3 Numerical Solution for Two-Module Gene Circuit

For the coupled mechanobiological gene circuit (in Section 1.2), we employed a numerical solver (Mathematica; version 9, Wolfram Research) to conduct kinetic and steady-state analyses. The outputs for the code below are found in Figure 3B (kinetics plot with $E = 0.4$, and steady-state plot). To obtain Figure 3C plots, we changed the value of J (in code; equivalent to $\tilde{\alpha}_3$ in Section 1.2) from 0 to 1.8. To obtain plots for the case of $E = 0.003$, we changed the upper limit of the **For** loop to $\mathrm{i} < 0.0031$.

```
test = Partition[
 Flatten[Reap[
   For[i = .003, i < .4, i = i + .05, Clear[a, b, h, g, s, L, l, m, M, J, j, t, x, y, A1, A2, E1, q, r
       ];
     a = 1.10; b = 5; g = 1.20; h = 5; x = .440; y = .44; J = 0; j = 1.1; q = 5; r = 1.20; s = 5;
         A1 = 2.0; A2 = 2.0; E1 = i; Ko = 9.2;
     s = NDSolve[{l'[t] == a*L[t] - b*l[t],
      L'[t] == g*l[t] - h*L[t]^A1/(M[t]^x + L[t]^A1),
      m'[t] == J*L[t] + j*M[t] - q*m[t],
      M'[t] == r*m[t] - s*M[t]^A2/(E1^y + M[t]^A2),
      l[0] == .005, L[0] == .005, m[0] == .005, M[0] == .005}, {l, L, m, M}, {t, 0, 1000}];
     Plot[Evaluate[{l[t], L[t], m[t], M[t]} /. s], {t, 0, 1000}, PlotRange -> {{0, 15}, {0.00001,
         1.1}}, PlotStyle -> Thick] Sow[{L[1000] /. s, l[1000] /. s, M[1000] /. s, m[1000] /. s
         }]];][[2, 1]]], 4]; Lss = test[[All, 1]]; lss = test[[All, 2]]; Mss = test[[All, 3]]; mss
         = test[[All, 4]];
Plot[Evaluate[{200 L[t], 200 M[t]} /. s], {t, 0, 100},P lotRange -> {{0, 25}, {0., 10}}, PlotStyle ->
    Thick, PlotLegends -> {"Lamin protein", "Myosin protein"}]
ListLogLogPlot[{Partition[Riffle[200 Lss, 200 Mss], 2]}, PlotRange -> {{0.5, 20}, {0.5, 20}}]
```

4 Numerical Solution for Tissue-level Coupled Gene Circuit

The code listed below refers to Section 1.3 on modeling of the mechano-regulated dynamics of collagen production (by cardiac fibroblasts) and myosin expression and hence contraction levels (by cardiomyocytes), which prints out Figure 5C:

```
Clear[a, b, h, g, u, s, F, f, M, m, J, j, t, T, x, y, k0]
a = 5.2; b = 5; g = 3; h = 6.5; x = .51; j = 4.1; q = 3; r = 1.5; s = 7;
A1 = 1.6; A2 = 3.7; y = .39; z = 2; k0 = .89;
s = NDSolve[{F'[t] == a*f[t]^(z - 1)/(k0^z + f[t]^z) - b*F[t],
    f'[t] == g*F[t] - h*f[t]^A1/(m[t]^x + f[t]^A1),
    M'[t] == j*m[t] - q*M[t],
    m'[t] == r*M[t] - u*m[t]^A2/(f[t]^y + m[t]^A2),
    F[0] == .00051, f[0] == 0.00051, M[0] == 0.011, m[0] == 0.011},
    {F, f, M, m}, {t, 0, 1000}];
LogPlot[Evaluate[{100 F[t], 100 f[t], 100 M[t], 100 m[t]} /. s], {t, 0.5, 1000},
        PlotRange -> {{0, 15}, {0.1, 100.}}]
```

References

[1] B. Schwanhausser, D. Busse, N. Li, G. Dittmar, J. Schuchhardt, J. Wolf, W. Chen, and M. Selbach. Global quantification of mammalian gene expression control. *Nature*, 473(7347):337–342, 2011.

[2] J. Swift, I. L. Ivanovska, A. Buxboim, T. Harada, P. C. D. P. Dingal, J. Pinter, J. D. Pajerowski, K. R. Spinler, J. W. Shin, M. Tewari, F. Rehfeldt, D. W. Speicher, and D. E. Discher. Nuclear lamin-a scales with tissue stiffness and enhances matrix-directed differentiation. *Science*, 341(6149):1240104, 2013.